Sensors & Actuators: A. Physical 358 (2023) 114447

Contents lists available at ScienceDirect

Sensors and Actuators: A. Physical

journal homepage: www.journals.elsevier.com/sensors-and-actuators-a-physical

Non-linear GMI decoding in 3D printed magnetic encoded systems

J.J. Beato-López [a,b,*], J.M. Algueta-Miguel [c,d], I. Galarreta-Rodriguez [a,b], E. Garaio [a,b], A. López-Ortega [a,b], C. Gómez-Polo [a,b], J.I. Pérez-Landazábal [a,b]

[a] Dpto. de Ciencias, Universidad Pública de Navarra, 31006 Pamplona, Spain
[b] Institute for Advanced Materials and Mathematics INAMAT2, Universidad Pública de Navarra, 31006 Pamplona, Spain
[c] Dpto. de Ingeniería Eléctrica, Electrónica y Comunicación, Universidad Pública de Navarra, 31006 Pamplona, Spain
[d] Institute for Smart Cities, Universidad Pública de Navarra, 31006 Pamplona, Spain

ARTICLE INFO

Keywords:
3D printing
Polymer-matrix composites
Three states encoding information
Non-linear GMI effect
Magnetic sensor
Magnetization direction reversal

ABSTRACT

The nonlinear giant magnetoimpedance (GMI) effect was explored as a highly sensitive sensing technology in 3D-printed magnetic encoded systems. Magnetic nanoparticles with low (magnetite, Fe_3O_4) and high (Co ferrite, $Co_{0.7}Fe_{2.3}O_4$) magnetic remanence were embedded (10 wt%) in a polymeric matrix of Polylactic Acid (PLA) and Poly-ε-caprolactone (PCL) and extruded in magnetic filaments to be 3D printed by the Fused Deposition Modelling technique (FDM). Two different geometries were constructed namely, individual magnetic strips and fixed barcoded pieces. The stray magnetic fields generated by the magnetic nanoparticles were detected through the non-linear (second harmonic) GMI voltage using a soft magnetic CoFeSiB wire as the nucleus sensor. The decoding response was analyzed as a function of the magnetization remanence of the nanoparticles, the distance between the individual magnetic strips, and the position (height) of the GMI decoding sensor. It has been shown that modification of the net magnetization direction of each individual fixed strip within the barcode geometry is possible through the application of local external magnetic fields. This possibility improves the versatility of the 3D binary encoding system by adding an additional state (0 without nanoparticles, 1 or −1 depending on the relative orientation of the net magnetization along the strips) during the codifying procedure.

1. Introduction

Magnetic materials display an outstanding role in the development and implementation of novel technologies [1, 2]. A clear example is their broad applicability in different technological fields such as consumer electronics, information storage, sensing, smart devices, energy conversion, etc. [3–7]. This wide range of applications requires the parallel development of novel fabrication procedures to satisfy the increasingly demanding requirements of new technologies. Furthermore, it becomes relevant the development of adequate manufacturing procedures that permit the design of complex geometries [8], precise control of structures at micro or nanometric scale [2], or the production of multifunctional materials with an optimized combination of mechanical and physical properties [9]. In this sense, some of the most commonly employed manufacturing processes, namely, injection molding [10, 11], casting [12, 13], and compaction [14] exhibit some limitations related to the energy consumption, necessity of post-manufacturing machining, complex geometries, expensive production techniques, or generation of waste materials, [8, 15, 16]. Thus, to overcome these constraints, the development of new manufacturing strategies to satisfy these demanding requirements is critical.

Additive Manufacturing (AM) has lately gained relevance in the design of novel (magnetic) materials due to its versatility [15], which relies on the possibility of high flexibility self-custom designs, rapid prototyping of complex geometries, and the combination of different materials, enabling the obtention of structures with unprecedented complexity and functionality [8, 17, 18]. This technology is able to produce 3D objects from an initial digital design by the deposition of successive printed layers [19]. Thus, AM is currently used in various technological sectors such as aerospace, biomedical, automotive, electronic devices, robotics, energy, etc. [9, 20-24]. Different techniques can be found within Additive Manufacturing techniques. Among them, Fusion Deposition Modeling (FDM) is one of the most utilized [25]. It consists of the injection of a molten polymer-based filament through a nozzle, by following a predetermined trajectory and forming

* Corresponding author at: Dpto. de Ciencias, Universidad Pública de Navarra, 31006 Pamplona, Spain.
E-mail address: juanjesus.beato@unavarra.es (J.J. Beato-López).

https://doi.org/10.1016/j.sna.2023.114447
Received 28 March 2023; Received in revised form 9 May 2023; Accepted 18 May 2023
Available online 20 May 2023

layer-by-layer the designed manufactured object geometry [25, 26]. The incorporation of active materials to the polymer-based filament, i.e. with magnetic properties, enables the manufacturing of complex multifunctional devices.

In a previous work, a proof of concept was demonstrated for the encoding-decoding of 3D printed information using the FDM technique. [27]. This procedure is based on the detection of the stray magnetic fields generated by the embedded magnetic nanoparticles (MNPs) employing the Giant Magnetoimpedance (GMI) effect [28]. However, further studies are required to comprehend and optimize the encoding-decoding procedure. Thus, in this work, the optimization of the device is approached from a double perspective. First, through the improvement of the detection sensitivity utilizing the non-linear (second harmonic, V_{2f}) components of the GMI voltage [29] in an optimized CoFeSiB amorphous wire. Secondly, through the appropriate selection of the embedded MNPs (magnetite or Co ferrite) and the configuration of the magnetic bands. Besides, the control of the net magnetization of each individual magnetic strip by local magnetic fields enlarges the binary coding capacity of the system. In this scenario, the proposed coded system can be integrated into the manufacturing process of the piece from the initial design stage, resulting in a one-step method. The embedded code hinders unauthorized replicas of the product, at the time that its decoding would enable, under a contactless procedure and without compromising their appearance, the 3D object identification (serial number, manufacturer…), recognition (owner data), location, and the provision of permissions to let or deny the execution of further specific actions (logistic, parcel delivery, etc), among others. Finally, the code can be incorporated in a wide range of 3D objects even with curved surfaces [30].

2. Materials and methods

2.1. MNPs: synthesis, structural and magnetic characterization

Commercial magnetite, Fe_3O_4, (50–100 nm Sigma Aldrich, 637106), and Co Ferrite ($Co_{0.7}Fe_{2.3}O_4$) nanoparticles synthesized by thermal decomposition of metal-organic precursors [31], were employed. Both samples display the characteristic X-ray diffractograms of a spinel structure (Bruker D8 ADVANCE diffractometer Fd-3 m, JPCDS nº 89–0691) with no trace of secondary phases. The crystallite sizes of the synthesized Co ferrite MNPs were estimated at around 21 ± 1 nm from the 400 diffraction peak (see Fig. S1) by means of Scherrer's equation. The magnetic response of both MNPs was characterized by a homemade Vibrating-sample magnetometer (VSM) under a maximum applied field of 1.5 T at room temperature. As expected, from its high magneto-crystalline anisotropy, Co ferrite nanoparticles display higher magnetization at the remanent state (~26 emu/g) compared to commercial magnetite particles (~5 emu/g). Besides, the hard magnetic nature of the Co ferrite is also reflected in the high coercive field values (see Fig. S2).

2.2. Fabrication of 3D printable filaments and pieces printing

Two different types of 3D printable magnetic filaments were produced employing both Fe_3O_4 and Co ferrite MNPs. To manufacture these filaments, the solution casting method was used [26]. Specifically, a concentration of 10 wt% of MNPs was embedded into a polymeric matrix composed of 90% Poly-ε-caprolactone (PCL) and 10% of Polylactic Acid (PLA). As a result, a precursor composite with a foam texture was obtained. The final 3D magnetic filaments were obtained by the extrusion (FelFil Evo extruder) of the precursor foams at a temperature of 80 ºC. A more detailed explanation of the whole process can be found in [27]. Prepared filaments were analogously magnetically characterized through the VSM. Table 1 summarizes the characteristic magnetic parameters for both initial MNPs and the 3D printable magnetic filaments (see Fig. S2 and Fig. S3). A decrease in the net magnetization of the filaments was found with respect to the initial MNPs due to the diminution of the magnetic fraction. The ratio between the saturation magnetization in both analyzed cases ($M_S^{MNPs}/M_S^{filament}$) is close to the nominal MNPs concentration (10 wt%). Negligible changes in the coercive field values, H_C, were detected in the extruded filaments indicating the absence of remarkable changes in the interparticle magnetic interactions after extrusion. Once again, higher remanence was found in the Co ferrite-based filament compared to the pure magnetite-based filament.

Table 1
Characteristic magnetic parameters for both initial MNPs and fabricated 3D printable magnetic filaments. Concretely, the coercive field H_C, saturation magnetization, M_S, and magnetization at the remanent state, M_r, are shown.

		H_C (Oe)	M_s (emu/g)	M_r (emu/g)	$M_S^{MNPs}/M_S^{filament}$
Fe_3O_4	MNPs	125	78.5	5.0	0.08
	Filament	125	6.5	0.45	
Co ferrite	MNPs	610	80.5	26.0	0.13
	Filament	610	10.5	4.1	

Then, using the FDM technique, both filaments were employed to design 3D-printed pieces. In particular, two different geometries were fabricated, on the one hand, individual magnetic strips (3D printer Sidewinder x1) consisting of independently printed rectangular bars 10 mm long, 1.5 mm wide, and 1 mm thick (Fig. 1a). This configuration allowed the modification of the distance, d, between the magnetic bands, from 1 to 9 mm. On the other hand, fixed barcodes (3D Raise 3D E2 printer with two print heads) made up of 6 strips with an alternating pattern of polymeric (state "0", 10 ×3×1 mm) and magnetic bands (" 1" or state "−1″, 10 ×2×1 mm). The width of the polymeric strips coincides with the fixed spacing distance (d = 3 mm) between magnetic bars (Fig. 1b). An example of each type of piece using the Co ferrite-based and magnetite-based filaments is shown in Fig. 1a and Fig. 1b, respectively. Analogous individual strips and barcoded pieces were also printed using the counterpart filament.

The Co ferrite printed pieces were initially pre-magnetized using an external magnetic field of 0.5 T (electromagnet Applied Magnetics Laboratory, 4H2 – 45) along the strip axis. The hard magnetic response of the embedded MNPs led to a constant remanence value with no time evolution. In contrast, the relaxation effects observed in pure magnetite MNPs allowed the analysis in two different situations, as-printed state and immediately after the application of a pre-magnetizing field of 0.1 T. Anyway, all scans were performed in the absence of any external magnetic field.

2.3. Comparison of first and second harmonic GMI voltages response

The decoding process is based on the detection of the stray magnetic

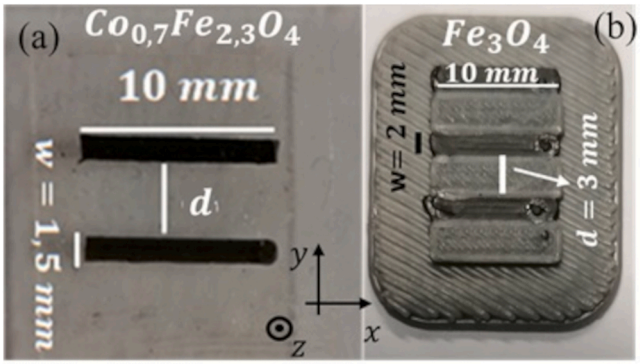

Fig. 1. 3D printed pieces: a) Co ferrite MNPs individual strips and b) magnetite 6 strips barcoded piece. Analogous pieces to those shown in a) and b) were printed for magnetite and Co ferrite MNPs respectively.

fields associated with the MNP embedded in the printed strips. A soft magnetic amorphous wire $(Co_{0.94}Fe_{0.06})_{72.5}Si_{12.5}B_{15}$ obtained by the "in-rotating-water-quenching" [32] technique was used as a nucleus sensor. Similarly to [27], a 5 cm in-length piece was submitted to a thermal-torsional treatment (t = 5 min, j = 19.5 A/mm^2 and torsional strain ξ= 10π rad/m) to improve its response in the low magnetic field region and enhance the non-linear terms (second harmonic), by inducing a helical anisotropy on the sample [33]. A piece of 10 mm was cut and fixed to a squared glass cover (side 15 mm and 0.2 mm in thickness) to ease its handling. As shown in [27], the optimal exciting conditions were found at a frequency of f= 100 kHz and peak-to-peak current intensity, I_{pp}= 20 mA. These conditions remained unaltered throughout the whole study.

Then, the detection capacities of the first, V_{1f}, and second harmonic GMI voltage, V_{2f}, were compared under the same experimental conditions. Both voltage variations, V_{if}; i = 1, 2, were registered along successive scans performed over the piece shown in Fig. 1a containing Co ferrite MNPs with higher remanence (data available in the supplementary section, Fig. S4). The sensor was located over a height z = 0.3 mm of the top piece surface to avoid physical contact between both elements and aligned in parallel to the individual magnetic strips axis along the x – direction. The scans along the y – direction were controlled through an adapted commercial 3D printer motor (Artillery Sidewinder x1) and LabView 2014 was employed both for the piece scanning and the acquisition of the harmonic voltage values, V_{if}, through the commercial lock-in amplifier (Stanford Research Systems SR 844) under a voltage divider configuration. To compare both GMI voltage signals, their experimented relative variations were calculated by the expression $\Delta V_{if} = \frac{V_{if}(y) - V_{ifmin}}{V_{ifmin}} x100$ where $V_{if}(y)$ is the voltage value at each y position and V_{ifmin} represents the lowest voltage value registered in each scan. Fig. 2 shows the evolution of ΔV_{if} as a function of the scanning distance, y, where the location and dimensions of the magnetic strips were drawn in grey. As previously reported [34], an enhanced response of V_{2f} was found (higher voltage variations under the effect of the magnetic field generated by the MNPs in the strips).

In view of the previous results, homemade electronics for the signal conditioning of V_{2f} was implemented in the final decoder system. The designed sensor interface is based on a "double phase lock-in amplifier" scheme, with an equivalent architecture to that described in [34]. The principle of operation relies on the employment of a two-phase frequency divider to generate two 200 kHz square signals with 90° of phase difference. One of the signals was used as a reference signal by the "implemented lock-in amplifier". The other signal was again frequency-divided an integrated to generate a triangular signal under

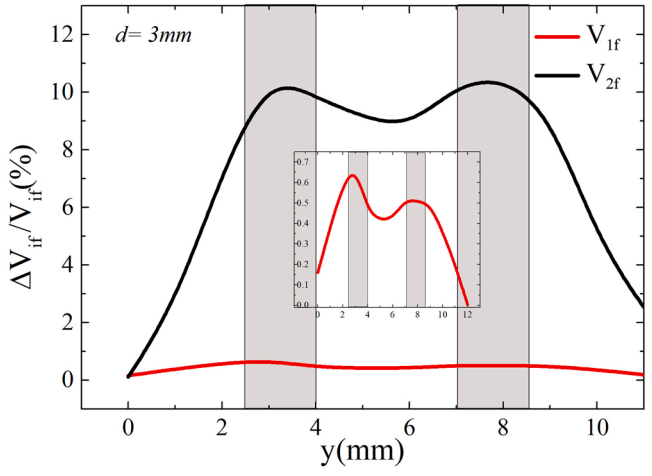

Fig. 2. Relative variation of the first, V_{1f}, and second V_{2f}, harmonic voltage versus sensor position, y. The scanned piece was formed by two magnetic strips embedded with Co ferrite MNPs separated d = 3 mm.

GMI optimal conditions. This signal excited the sensor, which was situated in the feedback loop of a transimpedance amplifier to assure an intermediate output voltage signal linear with the sensor impedance variations. Finally, the implemented "two-phase lock-in amplifier" provides two output DC voltages which were proportional to the phase and quadrature components of the second harmonic voltage respectively, whose root mean square permitted to obtain the final output signal V_{2fout}.

A characterization under controlled conditions was first addressed to calibrate the decoder system. So, the DC output signal, V_{2fout}, was evaluated (multimeter HP34401A) as a function of the magnetic field generated by the Helmholtz coils. As the inset of Fig. 3a shows, the largest sensitivity (slope of the curve) was found between − 260 and 260 A/m, although, a reduction of the sensor sensitivity was noticed around the zero magnetic field region. So, a bias magnetic field close to 150 A/m (V_{2fout} ~2.8 V) was applied to set the sensor operation point beyond that region (see the arrow in Fig. 3). It must be pointed out that the bias magnetic field was not strong enough to cause any change in the MNPs magnetization during the detection (scans) procedure (see Fig. S2 and S3). More interestingly, a linear behavior of the output signal characterizes the interval 140–170 A/m (2.7–3.1 V, see red line in Fig. 3) enabling the estimation of the device sensitivity in this range, i.e. 0.75 V/Am^{-1} (or 55 V/Oe). It must be remarked that a noticeable increment in sensitivity was achieved for V_{2f} compared with the value 2×10^{-3} V/Am^{-1} (or 0.16 V/Oe) found in [27] employing V_{1f}. The increase in sensitivity (two orders of magnitude) facilitated the detection of lower amounts of embedded MNPs, allowing a reduction in the dimensions of the codified pieces. Moreover, the selected operation point enabled to discriminate the direction of the stray magnetic field to be sensed since magnetic fields along the direction of the bias field resulted in V_{2fout} increment and vice versa.

After calibration, all printed pieces were scanned to study the influence in the decoding process of three main parameters, in order: i) the effect of decreasing the distance d, between individual magnetic strips, ii) the effect of increasing the height z (in both cases using the individual magnetic strip configuration); and iii) the feasibility of local and individual manipulation of the strips' magnetization direction (barcoded pieces) by the effect of a permanent magnet. In this last case, cylindrical ferrite magnet (0.1 T, 5 mm long, and 5 mm in diameter) for magnetite and NdFeB (0.4 T, 10 mm long, and 6 mm in diameter) for Co ferrite MNPs were used. Their magnetic field strengths were measured close to their surface. Although a decay in their strength occurred along the strip length, the magnetic field was strong enough to saturate the MNPs in the whole strip. All scans were performed as previously described, but incorporating the electronic interface for the excitation and signal conditioning of the sensor. It must be remarked that all pre-magnetizing fields were applied before the scanning of the pieces, being the scans performed in absence of a magnetic field (except the low-strength bias magnetic field for setting the sensor in the appropriate operation range).

3. Results and discussion

3.1. Effect of varying distance between individual magnetic strips

Fig. 4 shows the variation in the decoder output signal, V_{2fout}, as a function of the sensor position, y, under the two strips geometry (Fig. 1a) for both MNPs. Whereas for magnetite MNPs it is not necessary to pre-magnetize the coding strips, allowing their analysis in the as-printed state, Co ferrite particles required a previous pre-magnetization. Firstly, the largest distance between individual magnetic strips was analyzed, d = 7 mm and 9 mm for the as-printed Fe_3O_4 and Co ferrite, respectively (two grey bars in Fig. 4). Clear peaks centered at the strip positions were detected with an equivalent decrease of V_{2fout} at both sides of the maxima. This fact indicates a symmetric distribution of the stray magnetic field around the strips, revealing that the embedded MNPs would not magnetically interact due to the large distance between

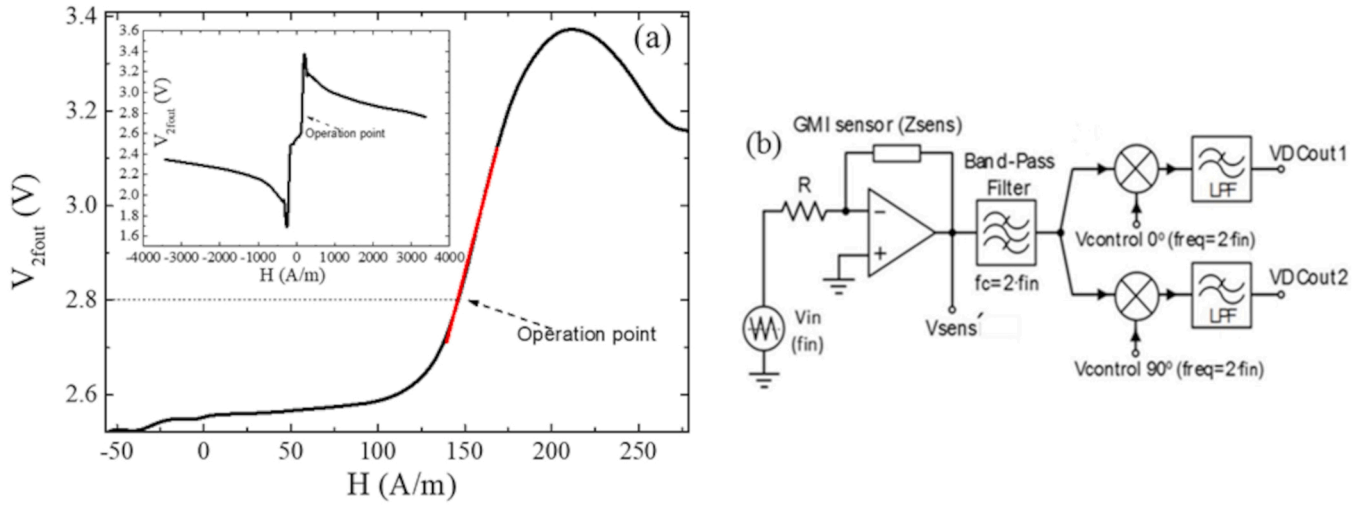

Fig. 3. (a) Variation of the electronic sensor interface output signal, V_{2fout}, versus the applied magnetic field H generated by Helmholtz coils in the operation region of the device. Inset. Complete calibration curve of the decoder system. (b) Schematics of the designed homemade electronics for the GMI sensor signal conditioning [27].

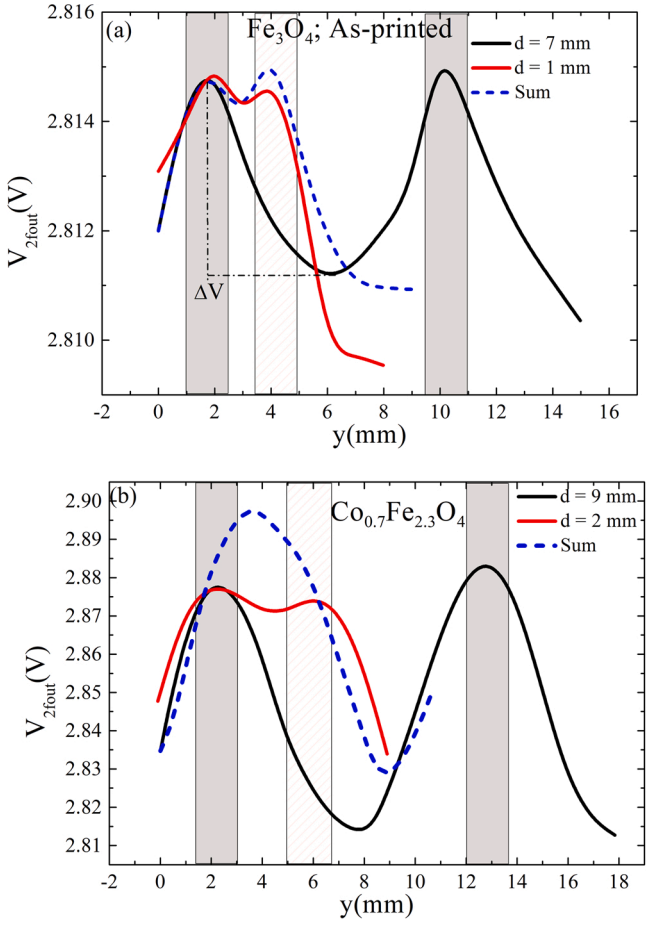

Fig. 4. Variation of the decoder output signal, V_{2fout}, versus sensor position, y, for extremal distances between individual magnetic strips in (a) as-printed magnetite and (b) Co ferrite-based pieces. The clearer bar represents the positions of the second magnetic bar for the lowest distance. In the dashed line the sum peak results from the addition between the initial detection peak and the second one (measured at extremal distances) after being mathematically translated to the lowest experimental analyzed distance.

the analyzed strips. The shown distances (7 and 9 mm) are the lowest that respectively fulfill this characteristic.

Then, successive scans were performed by sequentially approaching the second magnetic strip towards the initial fixed one. As d was reduced, the difference between the first voltage peak maximum and the minimum between magnetic strips, ΔV, decreased (see Fig. 4), reflecting the presence of an increasing magnetic field between the magnetic elements [27]. This process was repeated until the lowest distance where both strips could be independently detected through a voltage minimum at the middle distance between the strips. This situation is represented by the pale bar in Fig. 4 and corresponded to d = 1 mm for the as-printed magnetite-based and d = 2 mm for Co ferrite-based MNPs. It must be mentioned that all examined cases showed higher V_{2fout} variations in the Co ferrite based piece as a consequence of the strongest magnetic field generated by these nanoparticles.

The trend of ΔV is summarized in Fig. 5. A general decay was observed as the strips got closer (decreasing d) in such a way that the higher the magnetization in the strips the faster the decay. This trend may be the consequence of i) just the overlapping of the two detection peaks (algebraic sum of the magnetic field generated by each strip) when d was diminished or ii) its combined effect with magnetic

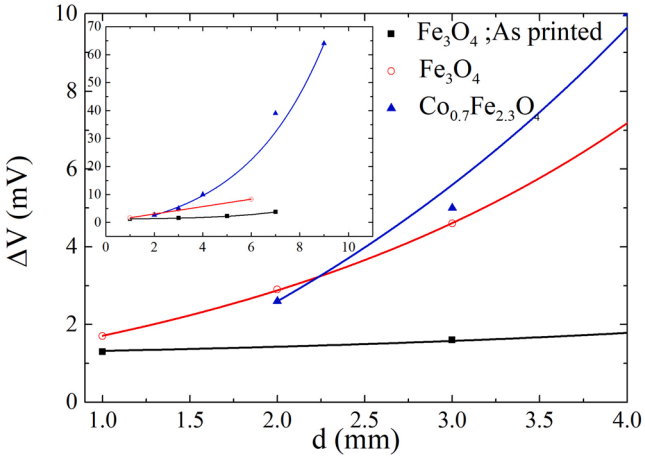

Fig. 5. Variation of the amplitude ΔV in the low distance, d, region for magnetite and Co ferrite MNPs based pieces. Inset: ΔV evolution in the whole range of analyzed distances.

interactions between strips. To elucidate this point, the second detection peak (maximum scanned distance), was fitted to a Gaussian function (although not physically realistic, this simple function was used as a rough approximation and only for illustration). The fitted peak was (mathematically) shifted towards the first strip peak (see dash peak in Fig. 4a and b) to simulate the lowest experimental distance measured situation. As can be deduced from Fig. 4, for the low remanence case, mutual interactions can be disregarded and the experimental sensor response is equivalent to the peak voltage sum. However, for the MNPs with higher remanence, the magnetostatic interactions modify the peak profile, leading to the occurrence of two peaks centered at the strip locations, instead of the single peak of the overlapping sum peak. Hence, the interaction between magnetic strips (actually the embedded Co ferrite MNPs) cannot be excluded.

As previously indicated, unlike Co ferrite MNPs, magnetite as-printed strips were detected without the necessity of applying a pre-magnetization field. Even in this situation, narrower detection peaks were found enabling a more localized strip detection. The magnetization (0.1 T) of the magnetite strips gave rise to a better definition of the signal peaks and a decrease in the peak widths. In fact, as Fig. 5 shows, ΔV displayed a remarkable increase after magnetizing the magnetic strips.

3.2. Effect of height on decoding stage

3D printing makes it possible to hide encoded information on a device by using a polymer top layer (thickness z) to cover the active material. Then, non-contact decoding processes using GMI magnetic sensors require the analysis of the detection efficiency as a function of the distance z between the active material and the sensor core. The study was performed in the most restrictive conditions, (d = 1 mm and d = 2 mm for as-printed magnetite and Co ferrite particles, respectively, Fig. 1a). As an example, Fig. 6a displays the output voltage at different z in the case of Co ferrite particles. As z increases a progressive decrease of ΔV was found. It is interesting to note that for large z, the sensor's lack of resolution led to a flat region, ΔV = 0, between magnetic strips. A similar behaviour was observed for as-printed magnetite particles (see Fig. S6)) but larger ΔV values were observed in Co ferrites MNPs at equivalent heights (Fig. 6b). This result should be linked to the higher remanence of Co ferrite MNPs (higher stray magnetic fields). Specifically, magnetite strips were detected up to z = 0.6 mm, while Co ferrite strips were detected until z = 1.1 mm. The larger interval available in the high remanence Co ferrite MNPs makes them more suitable for situations where considerable distances are required between the sensing element and the magnetic code.

3.3. Effect of magnetization reversal in barcoded pieces

Finally, the fixed barcoded pieces (geometry displayed in Fig. 1b) were employed to analyze the feasibility of manipulation of the net strips' magnetization direction and thus the possibility to increase the coding capability. Among other aspects, the possibility of the local and individual reversing process of the magnetization direction in each strip was addressed through the application of external magnetic fields generated by permanent magnets, concretely, a ferrite (0.1 T, 5 mm in length and 5 mm in diameter) and NdFeB magnet (0.4 T, 10 mm in length and 6 mm in diameter) for Fe_3O_4 and Co ferrite barcoded pieces, respectively. In both cases, the magnet was located at the beginning of each magnetic strip (x ≈ 0, see Fig. 1b) generating the magnetic field along the x- direction.

3.3.1. Fe_3O_4 MNPs

Fig. 7a shows the scanned voltage V_{2fout} for the magnetite piece in the as-printed state and after being pre-magnetized. The presence of two minima and maximum peaks in the position of the magnetic strips denotes a random direction of the net strip magnetization in the as-printed

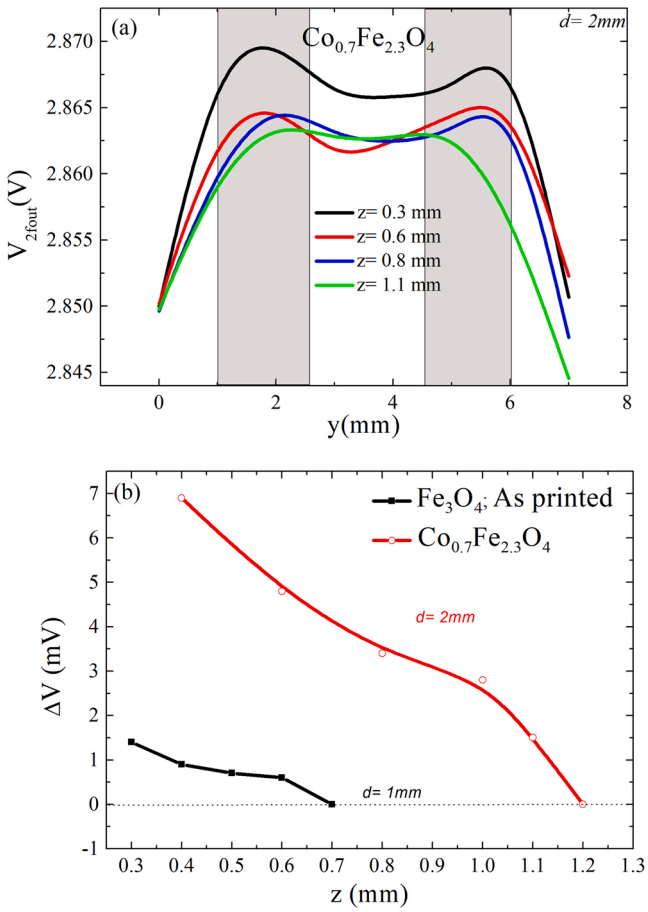

Fig. 6. Evolution of amplitude ΔV with the height, z, for the magnetite and Co ferrite piece.

state. The subsequently controlled pre-magnetization (applied field in the same direction) caused the appearance of three minima (Fig. 7a). These results corroborate the capacity to reverse the net magnetization of the magnetic strips through the application of an external magnetic field. Furthermore, as previously found in the former configuration, the pre-magnetization induces an increase in ΔV (see Fig. 7a) respecting the as-printed state. However, due to the superparamagnetic nature of a fraction of Fe_3O_4 MNPs, the occurrence of relaxation effects cannot be disregarded. In fact, once the pre-magnetization field was eliminated (t = 0), ΔV described a clear temporal evolution (Fig. 7b) observing a decay for t ≤ 10 min, followed by a stabilization at longer times. Notice that the measurements in the printed strips are taken immediately after removing the pre-magnetizing field (t ≈ 0). These relaxation effects can be considered detrimental for encoding and/or detection but the final stabilized state (t > > 10 min, i.e. Fe_3O_4 MNPs in remanence) permitted the strip detection in similar conditions than in the as-printed state (see Fig. 7a and Fig. S7).

In our previous work [27], the printed bands were employed as a binary encoding system, that is, "1" and "0" states where the direction of magnetization within the strip was disregarded. However, the possibility to separately pre-magnetize each strip would allow the incorporation into the encoding process of the "− 1" state associated with a specific direction of magnetization along the printed magnetic band. Hence, the initial encoding state displayed in Fig. 8 (three maxima) was locally changed by reverting the magnetization direction of the central magnetic strip. The presence of a single minimum at this strip position (Fig. 8) confirms the successful incorporation of the "− 1″ state. This outcome allows increasing the volume of information that can be stored in a given geometry, at the time that confers to the barcode the capacity

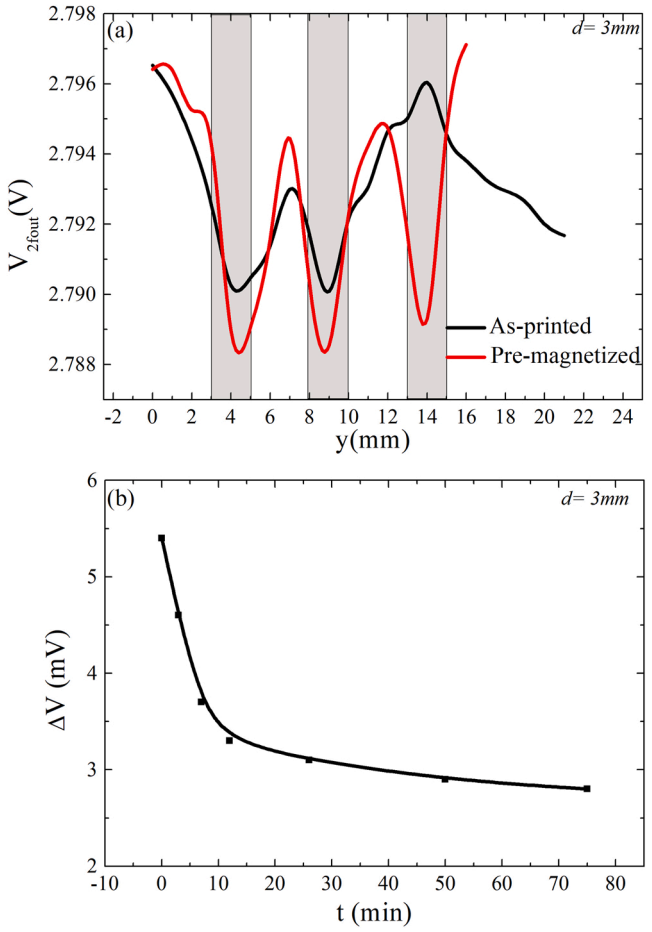

Fig. 7. (a) Variation of the decoder output signal, V_{2fout}, versus sensor position, y, for the as-printed magnetite piece and just after being magnetized (0.1 T). (b) Temporal dependence of ΔV.

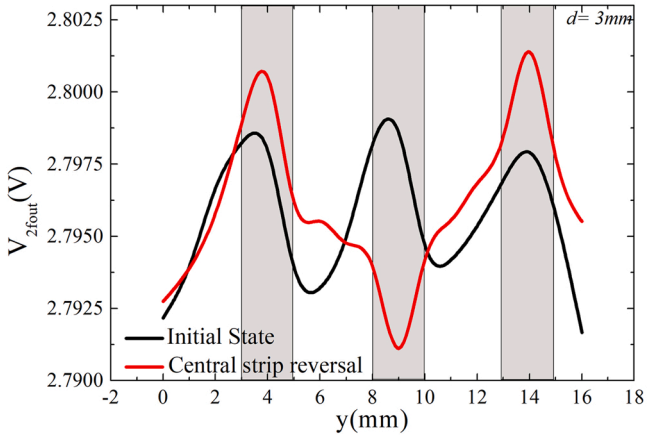

Fig. 8. Evolution of V_{2fout} versus sensor position, y, for a commom magnetization direction on all magnetite constituent magnetic strips and after locally reversing the magnetization direction of the central magnetic strip upon the application of the magnetic field 0.1 T. In both cases, the magnetic field was generated by a ferrite magnet.

of becoming programmable and reusable. Local reversal of the direction of magnetization of the end strips is equally feasible (Fig. S8).

3.3.2. $Co_{0.7}Fe_{2.3}O_4$ MNPs

In a parallel way, the same analysis was carried out with the high-remanence Co ferrite MNPs. The higher coercivity of Co ferrite MNPs (see Table 1) requires the application of stronger magnetic fields to manipulate the direction of magnetization (NdFeB cylindrical magnet). As Fig. 9 shows, the controlled reversal of the magnetization direction of the strips was also demonstrated. As an example, the change in magnetization of the central magnetic strip is shown, although all other combinations were also tested (Fig. S 9).

Although both systems allow versatile ad-hoc modifiable coding which can be read in absence of an externally applied magnetic field, some relevant differences can be highlighted. In particular, the piece based on Co ferrite did not show any time evolution and experienced higher amplitudes after magnetization reversal, although at the expense of a noticeable broadening of the detection peaks with respect to the starting configuration. This points towards a more complex inversion process (use of rare-earth-based magnets) than in the case of magnetite particles, resulting in a more delocalized detection of the strip position, requiring larger distances between adjacent strips for their independent detection.

In summary, it can be concluded that magnetite-based strips show a better encode-decode response due to: i) the state can be detected even in the absence of pre-magnetization (ready-to-use), ii) narrower detection peaks were observed facilitating spatially localized detection, and iii) a simpler manipulation of the magnetization direction, not requiring rare earth magnets. Successful control of the magnetization direction is compulsory to improve the coded-decoded system through the incorporation of the "– 1″ state. Specifically, the amount of combinations that can be implemented in the three-state coded element is increased in a factor $(3/2)^N$ (where N is the number of pieces of the barcode) compared to a two-state or binary codification system [35]. In these terms, the output state will be determined by dividing the total voltage swing of the sensor into three different regions, in turn, separated by two threshold voltages. Hence, the upper region will be defined around the voltage maxima (V_1), corresponding to "1″. Similarly, the lower region around the voltage minima (V_{-1}) will be associated with "– 1″, and finally the middle region centered at the intermediate voltage, V_0, will be assigned to "0". To start the decoding process an initial "1″ state is considered. From its center, the GMI sensor is displaced until the central region of the next strip, where the output voltage signal is measured and compared with the threshold values to determine the bar state. This process is repeated until the total scanning of the embedded code. To minimize decoding errors, both threshold voltages must be properly set to define optimal confidence intervals, which may depend on the different strip features (dimensions, concentration and type of MNPs,

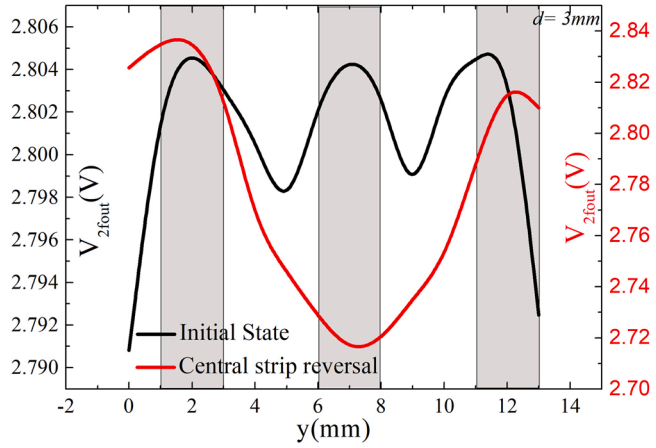

Fig. 9. Evolution of V_{2fout} versus sensor position, y, for commom magnetizatin direction on all Co ferrite constituent magnetic strips and after locally reversing the magnetization direction of the central magnetic strip upon the application of the magnetic field 0.4 T. In both cases, the magnetic field was generated by a NdFeB magnet. Note the different scales utilized in this figure.

etc). Additionally, the manipulation of the magnetization direction also provides tunability and reusability since the code can be magnetically reprogrammed, hindering the information reading by an unauthorized receiver, although still no possible modification of the state "0" can be performed. Finally, the availability of commercial magnetite particles makes them more suitable for additive manufacturing (3D printing) at the industrial level.

4. Conclusions

The nonlinear GMI effect has been explored for the detection and decoding of encoded magnetic information in 3D-printed polymeric barcodes. Two different geometries were printed from 3D filaments with low (magnetite) and high (co-ferrite) magnetic remanence nanoparticles. In both cases, the manipulability of the encoding through external magnetic fields was analyzed.

The best detection capability of the second harmonic has been demonstrated by direct comparison with the fundamental under the same experimental conditions (simple voltage divider configuration). The better performance is reflected in the fact that pieces with a lower amount of MNP can be used.

Magnetite nanoparticles can be detected without pre-magnetization. In addition, they show sharper detection peaks that allow individualized detection of strips at lower separation distances. The incorporation of the "– 1" state required a simpler manipulation of the direction of magnetization process and with narrower detection peaks allowing to increase the amount of information stored and its reprogrammability.

On the contrary, Co ferrite MNPs require a pre-magnetization stage, although their higher remanence favors their detection at greater distances, which could be of interest in certain specific applications where the sensor-bar code distance cannot be properly reduced.

These properties, together with the possibility of magnetic programmability of the barcode, result in a versatile, reusable, and tunable encoding-decoding process.

CRediT authorship contribution statement

Juan Jesús Beato López: Conceptualization, Methodology, Measurements, Validation, Formal analysis, Investigation, Data curation, Writing – original draft, Writing – review & editing. **José María Algueta Miguel:** Development of electronic interface, Writing – review & editing. **Itziar Galarreta Rodriguez:** 3D filament design, fabrication and characterization, Writing – review & editing. **Eneko Garaio:** 3D filament design and characterization, Software. **Alberto López Ortega:** 3D filament design, fabrication and characterization. **Cristina Gómez Polo:** Data curation, Formal analysis, Writing – original draft, Writing – review & editing. **Ignacio Pérez de Landazábal**: Conceptualization, Methodology, Validation, Resources, Funding acquisition, Project administration, Writing – review & editing.

Declaration of Competing Interest

The authors declare that they have no known competing financial interests or personal relationships that could have appeared to influence the work reported in this paper.

Data Availability

No data was used for the research described in the article.

Acknowledgments

This work has been funded by the Gobierno de Navarra - Departamento de Desarrollo Económico within the framework of the Project: "Advanced Manufacturing of Electronics, AMELEC". It has also been partially funded by the Spanish Government - Ministerio Ciencia - Innovación (PID2019–107258RB-C32 of MCIN/AEI/10.13039/501100011033) and from the grant PID2021–122613OB-I00 funded by MCIN/AEI/ 10.13039/501100011033. Open access funding is provided by Universidad Pública de Navarra. The authors also want to acknowledge the Technological Center specialized in mobility and mechatronics of Navarra (NAITEC), for supplying the 3D printed piece and Prof. M. Vázquez (ICMM, Madrid Spain) for kindly supplying the soft magnetic wires.

Appendix A. Supporting information

Supplementary data associated with this article can be found in the online version at doi:10.1016/j.sna.2023.114447.

References

[1] H. Szymczak, Magnetic Materials and Applications, in: F. Bassani, G.L. Liedl, P. Wyder (Eds.), Encyclopedia of Condensed Matter Physics, Elsevier, Oxford, 2005, pp. 204–211, https://doi.org/10.1016/B0-12-369401-9/00523-4.
[2] G. Florio, Applications of Magnetic Materials, in: A.-G. Olabi (Ed.), Encyclopedia of Smart Materials, Elsevier, Oxford, 2022, pp. 24–31, https://doi.org/10.1016/B978-0-12-815732-9.00067-X.
[3] O. Gutfleisch, M.A. Willard, E. Brück, C.H. Chen, S.G. Sankar, J.P. Liu, Magnetic materials and devices for the 21st century: stronger, lighter, and more energy efficient, Adv. Mater. vol. 23 (7) (2011) 821–842, https://doi.org/10.1002/adma.201002180.
[4] C. Tannous and R.L. Comstock, Magnetic Information-Storage Materials, in Springer Handbook of Electronic and Photonic Materials, S. Kasap and P. Capper, Eds., in Springer Handbooks. Cham: Springer International Publishing, 2017, pp. 1–1. doi: 10.1007/978–3-319–48933-9_49.
[5] A. Nakhlband, H. Kholafazad-Kordasht, M. Rahimi, A. Mokhtarzadeh, J. Soleymani, Applications of magnetic materials in the fabrication of microfluidic-based sensing systems: recent advances, Microchem. J. vol. 173 (2022), 107042, https://doi.org/10.1016/j.microc.2021.107042.
[6] Y. Kim, X. Zhao, Magnetic soft materials and robots, Chem. Rev. vol. 122 (5) (2022) 5317–5364, https://doi.org/10.1021/acs.chemrev.1c00481.
[7] Y. Song, K.P. Bhatti, V. Srivastava, C. Leighton, R.D. James, Thermodynamics of energy conversion via first order phase transformation in low hysteresis magnetic materials, Energy Environ. Sci. vol. 6 (4) (2013) 1315–1327, https://doi.org/10.1039/C3EE24021E.
[8] X. Wei, M.-L. Jin, H. Yang, X.-X. Wang, Y.-Z. Long, Z. Chen, Advances in 3D printing of magnetic materials: fabrication, properties, and their applications, J. Adv. Ceram. vol. 11 (5) (2022) 665–701, https://doi.org/10.1007/s40145-022-0567-5.
[9] V. Chaudhary, S.A. Mantri, R.V. Ramanujan, R. Banerjee, Additive manufacturing of magnetic materials, Prog. Mater. Sci. vol. 114 (2020), 100688, https://doi.org/10.1016/j.pmatsci.2020.100688.
[10] B.S. Zlatkov, et al., Properties of MnZn ferrites prepared by powder injection molding technology, Mater. Sci. Eng.: B vol. 175 (3) (2010) 217–222, https://doi.org/10.1016/j.mseb.2010.07.031.
[11] Y. Ye, et al., Effect of microcrystalline wax on the solvent debinding of the Sr-ferrite ceramics prepared by powder injection molding, J. Eur. Ceram. Soc. vol. 37 (5) (2017) 2105–2114, https://doi.org/10.1016/j.jeurceramsoc.2016.12.026.
[12] A. Wonisch, P. Polfer, T. Kraft, A. Dellert, A. Heunisch, A. Roosen, A comprehensive simulation scheme for tape casting: from flow behavior to anisotropy development, J. Am. Ceram. Soc. vol. 94 (7) (2011) 2053–2060, https://doi.org/10.1111/j.1551-2916.2010.04358.x.
[13] G. Jian, D. Zhou, J. Yang, Q. Fu, Tape casting of cobalt ferrite from nonaqueous slurry, J. Magn. Magn. Mater. vol. 324 (24) (2012) 4179–4183, https://doi.org/10.1016/j.jmmm.2012.07.042.
[14] M. Saura-Múzquiz, et al., Improved performance of SrFe12O19 bulk magnets through bottom-up nanostructuring, Nanoscale vol. 8 (5) (2016) 2857–2866, https://doi.org/10.1039/C5NR07854G.
[15] E.A. Périgo, J. Jacimovic, F. García Ferré, L.M. Scherf, Additive manufacturing of magnetic materials, Addit. Manuf. vol. 30 (2019), 100870, https://doi.org/10.1016/j.addma.2019.100870.
[16] A. Sarkar, M.A. Somashekara, M.P. Paranthaman, M. Kramer, C. Haase, I. C. Nlebedim, Functionalizing magnet additive manufacturing with in-situ magnetic field source, Addit. Manuf. vol. 34 (2020), 101289, https://doi.org/10.1016/j.addma.2020.101289.
[17] N. Martelli, et al., Advantages and disadvantages of 3-dimensional printing in surgery: a systematic review, Surgery vol. 159 (6) (2016) 1485–1500, https://doi.org/10.1016/j.surg.2015.12.017.
[18] C. Zhang, et al., 3D printing of functional magnetic materials: from design to applications, Adv. Funct. Mater. vol. 31 (34) (2021) 2102777, https://doi.org/10.1002/adfm.202102777.
[19] M.K. Thompson, et al., Design for additive manufacturing: trends, opportunities, considerations, and constraints, CIRP Ann. vol. 65 (2) (2016) 737–760, https://doi.org/10.1016/j.cirp.2016.05.004.

[20] U.M. Dilberoglu, B. Gharehpapagh, U. Yaman, M. Dolen, The role of additive manufacturing in the era of industry 4.0, Procedia Manuf. vol. 11 (2017) 545–554, https://doi.org/10.1016/j.promfg.2017.07.148.
[21] P. Bartolo, et al., Biomedical production of implants by additive electro-chemical and physical processes, CIRP Ann. vol. 61 (2) (2012) 635–655, https://doi.org/10.1016/j.cirp.2012.05.005.
[22] T. Pham, P. Kwon, and S. Foster, Additive Manufacturing and Topology Optimization of Magnetic Materials for Electrical Machines—A Review, Energies, vol. 14, no. 2, Art. no. 2, Jan. 2021, doi: 10.3390/en14020283.
[23] V. Juechter, M.M. Franke, T. Merenda, A. Stich, C. Körner, R.F. Singer, Additive manufacturing of Ti-45Al-4Nb-C by selective electron beam melting for automotive applications, Addit. Manuf. vol. 22 (2018) 118–126, https://doi.org/10.1016/j.addma.2018.05.008.
[24] L. Li, B. Post, V. Kunc, A.M. Elliott, M.P. Paranthaman, Additive manufacturing of near-net-shape bonded magnets: Prospects and challenges, Scr. Mater. vol. 135 (2017) 100–104, https://doi.org/10.1016/j.scriptamat.2016.12.035.
[25] M. Ralchev, V. Mateev, and I. Marinova, Magnetic Properties of FFF/FDM 3D Printed Magnetic Material," in 2021 17th Conference on Electrical Machines, Drives and Power Systems (ELMA), Jul. 2021, pp. 1–5. doi: 10.1109/ELMA52514.2021.9503037.
[26] E.M. Palmero, et al., Composites based on metallic particles and tuned filling factor for 3D-printing by fused deposition modeling, Compos. Part A: Appl. Sci. Manuf. vol. 124 (2019), 105497, https://doi.org/10.1016/j.compositesa.2019.105497.
[27] J.J. Beato-López, et al., Magnetic binary encoding system based on 3D printing and GMI detection prototype, Sens. Actuators A: Phys. vol. 347 (2022), 113946, https://doi.org/10.1016/j.sna.2022.113946.
[28] M.-H. Phan and H.-X. Peng, Giant magnetoimpedance materials: Fundamentals and applications, Progress in Materials Science, vol. 53, no. 2, Art. no. 2, Feb. 2008, doi: 10.1016/j.pmatsci.2007.05.003.
[29] C. Gómez-Polo, M. Vázquez, M. Knobel, Field dependence of second-harmonic amplitude of magnetoimpedance in FeCoSiB joule heated wires, J. Magn. Magn. Mater. vol. 226–230 (2001) 712–714, https://doi.org/10.1016/S0304-8853(00)01145-8.
[30] V. Iyer, J. Chan, and S. Gollakota, 3D printing wireless connected objects, ACM Trans. Graph., vol. 36, no. 6, p. 242:1–242:13, Nov. 2017, doi: 10.1145/3130800.3130822.
[31] A. López-Ortega, E. Lottini, C. de, J. Fernández, C. Sangregorio, Exploring the magnetic properties of cobalt-ferrite nanoparticles for the development of a rare-earth-free permanent magnet, Chem. Mater. vol. 27 (11) (2015) 4048–4056, https://doi.org/10.1021/acs.chemmater.5b01034.
[32] P. Sarkar, R.K. Roy, A.K. Panda, A. Mitra, Optimization of process parameters for developing FeCoSiB amorphous microwires through in-rotating-water quenching technique, Appl. Phys. A vol. 111 (2) (2013) 575–580, https://doi.org/10.1007/s00339-012-7260-4.
[33] C. Gómez-Polo, M. Vázquez, and M. Knobel, Rotational giant magnetoimpedance in soft magnetic wires: Modelization through Fourier harmonic contribution, Appl. Phys. Lett., vol. 78, no. 2, Art. no. 2, Jan. 2001, doi: 10.1063/1.1336814.
[34] J.J. Beato-López, J.M. Algueta-Miguel, C. Gómez-Polo, Contactless magnetic nanoparticle detection platform based on non-linear GMI effect, Measurement vol. 180 (2021), 109602, https://doi.org/10.1016/j.measurement.2021.109602.
[35] S.S. Haykin. Communication Systems, fourth ed., Wiley, New York, 2001.

J. J. Beato-López was born in Jerez de la Frontera, Spain. He received an M.Sc. degree from the University of Cádiz, Spain, in 2011. Then in 2018, he received his Ph.D. degree in physics (materials science) from the Public University of Navarre, Pamplona, Spain, where he became a Doctor Assistant Professor. His main research interests are related to the study of magnetic properties in materials and their application to the design of sensors.

José María Algueta Miguel received the Telecommunications Engineering and Ph.D. degrees from the Public University of Navarra, Spain, in 2008 and 2012 respectively. Currently, he is a researcher with the same university. He has been an invited researcher with the University College Dublin (UCD), Dublin, Ireland, in 2011, with the New Mexico State University, Las Cruces (NM), USA, in 2013, and with the INAOE, Puebla, Mexico, in 2015. His main research interests are related to low-power low-voltage analog design, mixed-mode electronic systems and sensor interfaces.

I. Galarreta-Rodriguez was born in Pamplona, Spain. She received an M.Sc. degree from the University of the Basque Country, Spain, in 2016. Then in 2022, he received the Ph.D. degree in Material Science and Technology from the University of the Basque Country, Bilbao, Spain. Her research interest are related to the preparation and study of magnetic nanomaterials and printable magnetic composites.

Eneko Garayo Urabayen was born in Pamplona, Navarre. He completed his degree in Physics at the Public University of Basque Country (UPV/EHU) in 2009. Afterwards, in 2015, he obtained his Ph. D. presenting a doctoral thesis entitled "Development of experimental techniques for magnetic hyperthermia therapy". In 2017 he started working as Doctor Assistant Professor at the Public University on Navarre (UPNA). His main research interests are related to the study of magnetic properties in nanoparticles and their applications.

Alberto López-Ortega was born in Barcelona, Spain. He received the bachelor degree in Chemical Science from the Universitat de Barcelona, Spain, in 2007 and the Ph.D. in Material Science from the Universitat Autònoma de Barcelona, Spain, in 2012. After three postdoctoral contracts (Italy and Spain) he joined the Public University of Navarre in 2020 becoming an associate professor in 2022. His research lines are based on the development of new nanostructured magnetic materials to address current technological requirements, highlighting both the study of the mechanisms that govern their growth process and their fundamental properties.

Cristina Gómez-Polo was born in Madrid, Spain. She received the M.Sc. and the Ph.D. degrees in Physics (Material Science) from the Complutense University, Madrid, Spain, in 1988 and 1992, respectively. In 1995 she joined the Public University of Navarre as a lecturer and become full professor in 2011. Her research activity is mainly focused on the magnetic properties and applications of nanostructured magnetic materials and includes the study of amorphous, nanocrystalline and nanoparticle systems.

J.I. Pérez-Landazábal was born in Vitoria-Gasteiz, Spain and received the Ph.D. degree in solid-state physics from the Basque Country University in 1995. He is full Professor in the Science Department of the Public University of Navarra, Pamplona, Spain and researcher of the Institute for Advanced Materials and Mathematics (InaMat^2). His research interests include ferromagnetic shape memory alloys, magnetic sensors and actuators and magnetic nanoparticles for medical applications. Nowadays, his activity is mainly focused on microstructural and magnetic characterization, phase transformations and defects in solids.